HHS Public Access

Author manuscript

Cancer Discov. Author manuscript; available in PMC 2018 April 01.

Published in final edited form as:

Cancer Discov. 2017 October ; 7(10): 1184–1199. doi:10.1158/2159-8290.CD-17-0250.

Blimp1 induces transient metastatic heterogeneity in pancreatic cancer

Shin-Heng Chiou[1], **Viviana I. Risca**[1], **Gordon X. Wang**[2], **Dian Yang**[1,3], **Barbara M. Grüner**[1], **Arwa S. Kathiria**[1], **Rosanna K. Ma**[1], **Dedeepya Vaka**[4], **Pauline Chu**[4], **Margaret Kozak**[5], **Laura Castellini**[6], **Edward E. Graves**[3,5,6], **Grace E. Kim**[7], **Philippe Mourrain**[2], **Albert C. Koong**[3,5,6], **Amato J. Giaccia**[3,5,6], and **Monte M. Winslow**[1,3,4,5,*]

[1]Department of Genetics, Stanford University School of Medicine, Stanford, CA, USA

[2]Department of Psychiatry and Behavioral Sciences, Stanford University School of Medicine, Stanford, CA, USA

[3]Cancer Biology Program, Stanford University School of Medicine, Stanford, CA, USA

[4]Department of Pathology, Stanford University School of Medicine, Stanford, CA, USA

[5]Stanford Cancer Institute, Stanford University School of Medicine, Stanford, CA, USA

[6]Department of Radiation Oncology, Stanford University School of Medicine, Stanford, CA, USA

[7]Department of Pathology, University of California San Francisco, San Francisco, CA, USA

Abstract

Pancreatic ductal adenocarcinoma (PDAC) is one of the most metastatic and deadly cancers. Despite the clinical significance of metastatic spread, our understanding of molecular mechanisms that drive PDAC metastatic ability remains limited. Using a novel genetically engineered mouse model of human PDAC, we uncover a transient subpopulation of cancer cells with exceptionally high metastatic ability. Global gene expression profiling and functional analyses uncovered the transcription factor Blimp1 as a key driver of PDAC metastasis. The highly metastatic PDAC subpopulation is enriched for hypoxia-induced genes and hypoxia-mediated induction of Blimp1 contributes to the regulation of a subset of hypoxia-associated gene expression programs. These findings support a model in which up-regulation of Blimp1 links microenvironmental cues to a metastatic stem cell character.

Keywords

Blimp1; PDAC; hypoxia; cancer metastasis; tumor heterogeneity

[*]Corresponding Author: Monte M Winslow, Stanford University School of Medicine, Mail code: 5120; 279 Campus Dr., Beckman Center, Stanford, CA 94305. Phone: (650) 725-8696. mwinslow@stanford.edu.

Additional information: The authors declare no competing financial interests.

Accession number: The accession number for all the next generation sequencing data is included in the following superseries: GSE90825.

Supplementary Data: Supplementary Data includes Supplementary Methods, thirteen Supplementary Figures, and three Supplementary Tables.

Introduction

PDAC is an almost uniformly lethal cancer that is projected to become the second leading cause of cancer-related deaths in the United States by 2030 (1). Most PDAC patients die from metastatic disease, underscoring the need to better understand the molecular mechanisms that drive disease progression and metastasis (2). Genomic analyses of PDAC have uncovered oncogenic *KRAS* and loss of function mutations in the *CDKN2A, SMAD4*, and *TP53* tumor suppressors as key recurrent drivers of pancreatic cancer development (3-6). While these studies have also offered clues about metastatic progression, they have not uncovered consistent genetic alterations that explain the progression to a highly metastatic state (7-10).

While genomic alterations create stable changes that increase cancer growth, transient alterations in the metastatic state of cancer cells can be induced by interactions with stromal cells, diverse physical cues, as well as by changes in the local tumor microenvironment. For example, the epithelial-to-mesenchymal transition (EMT) is a well characterized transcriptional program that endows cancer cells with a transient high metastatic ability (11). However, EMT might not be critical for PDAC dissemination or metastasis (12,13). Subpopulations of PDAC cells with cancer stem cell-like properties have also been described but it is unclear whether these cells are the major source of metastases (14,15).

In many cancer types, metastasis is thought to be driven by diverse extracellular cues that increased stem-like behavior as well as invasion and metastasis (16). PDAC in particular has an extensive desmoplastic stromal response that generates unique physical properties, including increased extracellular matrix stiffness and areas with limited oxygen and nutrient availability (17). However, whether or not PDAC metastasis is driven by features of the tumor microenvironment is unclear. Identification of key environmental factors could provide insights into the process of metastasis as well as aid in the development of novel therapeutic strategies.

Genetically engineered mouse models of PDAC recapitulate key genetic events of the human disease. Cre-mediated expression of oncogenic $Kras^{G12D}$ in pancreatic cells of *loxP-Stop-loxP* $Kras^{G12D}$ knock-in mice ($Kras^{LSL\text{-}G12D/+}$) leads to the development of early stage pancreatic intraepithelial neoplasms (PanINs) (18). Concomitant expression of point mutant *p53* or deletion of *p53*, *Cdkn2a*, and/or *Smad4* allows for the development of PDAC that can progress to gain multi-organ metastatic ability (19-23). Importantly, tumors arise *in vivo* from genetically defined lesions and evolve in their native context, providing the opportunity to identify the cancer cell intrinsic and extrinsic processes that contribute to tumor progression.

Here, we developed a novel mouse model of human PDAC, which enabled the isolation and molecular characterization of a highly metastatic subpopulation of pancreatic cancer cells. We demonstrate that these highly metastatic cancer cells exists within hypoxic tumor areas and that the transcription factor Blimp1 drives their high metastatic potential. Gene expression signatures of the metastatic state, as well as of hypoxia-induced Blimp1-dependant genes predicts PDAC patient outcome. These findings highlight

microenvironment-induced heterogeneity as a driver of pancreatic cancer progression toward its deadly metastatic phase.

Results

Generation of a system to identify and isolate a highly metastatic population of PDAC cells

The chromatin-associated protein HMGA2 is a marker of increased malignancy in many tumor types, and high HMGA2 expression predicts poor prognosis in several major human cancer types, including PDAC (24-30). To determine whether neoplastic cells in genetically engineered mouse models of human PDAC also express Hmga2, we performed immunohistochemistry (IHC) on tumors at different stages of development. Hmga2 was not expressed in cells in the normal adult pancreas or PanINs in *Kras*$^{LSL\text{-}G12D}$;*p53*$^{LSL\text{-}R172H/+}$;*Pdx1-Cre* (*KPC*) mice, but was expressed in a subset of PDAC cells (Supplementary Fig. S1A and data not shown). In human PDAC, HMGA2 expression correlates with metastasis to lymph nodes and poor prognosis, and we confirmed that high HMGA2 expression in PDAC patients predicts shorter survival (Supplementary Fig. S1B-S1D) (28,31). Together, these results document the expression of Hmga2 in a subset of cancer cells in mouse models of PDAC and confirm the correlation of the presence of cancer cells in the HMGA2^{pos} state with poor PDAC patient outcome.

To uncover the cellular and molecular features of Hmga2^{positive} and Hmga2^{negative} cancer cells, we generated a mouse model that would allow the isolation of these PDAC cell sub-populations. We incorporated two additional alleles into the *KPC* mouse model: a Cre-reporter allele (*R26*$^{LSL\text{-}Tomato}$) to fluorescently mark all neoplastic cells, and an *Hmga2* knock-in allele, which is converted by Cre from its wild-type conformation (*Hmga2*^{CK}) into a GFP reporter (*Hmga2*^{GFP}; Fig. 1A) (20,32). In the heterozygous state (*Hmga2*$^{CK/+}$), the potential for GFP expression is restricted to cells in which Cre has inverted a lox-flanked region and GFP expression remains under control of all endogenous *Hmga2* regulatory elements (20). In *KPC;R26*$^{LSL\text{-}Tomato/+}$;*Hmga2*$^{CK/+}$ mice (referred to as *KPC*^{colors} mice), all cancer cells were Tomato positive and Hmga2-expressing cancer cells were both Tomato and GFP positive (Supplementary Fig. S1A and S1E).

The dual fluorescent marking of cancer cells in *KPC*^{colors} mice provided us with the ability to isolate Tom^{pos}GFP^{neg} and Tom^{pos}GFP^{pos} cancer cells by fluorescence-activated cell sorting (FACS) (Supplementary Fig. S1F-S1G). Consistent with Hmga2 expression observed by IHC, variable percentages of cancer cells in individual tumors were GFP^{pos} (Fig. 1B-1C). In the *KPC* model, progression from PanINs to adenocarcinoma is driven by loss of the wild-type *p53* allele (19). Tom^{pos}GFP^{neg} and Tom^{pos}GFP^{pos} samples contained less than 10% remaining *p53*^{wt} allele and loss of the *p53*^{wt} allele led to the stabilization of mutant p53 protein in both GFP^{neg} and GFP^{pos} cells (Supplementary Fig. S1H-S1J). Thus, Tom^{pos}GFP^{neg} and Tom^{pos}GFP^{pos} cells represent two distinct sub-populations of pancreatic cancer cells.

We next performed cell culture and transplantation-based *in vivo* metastasis assays on GFP^{neg} and GFP^{pos} PDAC cells. GFP^{pos} cells consistently formed more spheres when plated into ultralow-attachment plates and formed more colonies when plated at low density under

standard tissue culture conditions (Supplementary Fig. S1K and data not shown). Most importantly, for eight out of eight tumors from *KPC*^{colors} mice, the GFP^{pos} PDAC cells formed more metastases than their GFP^{neg} counterparts when transplanted intravenously into recipient mice (Fig. 1D-1F). On average, GFP^{pos} cells were more than 10 times more metastatic than GFP^{neg} cells (p-value < 0.008; Fig. 1F). Interestingly, the tumors that arose from GFP^{pos} cells almost always had heterogeneous GFP expression, suggesting that GFP^{pos} cells may be in a transient state with the potential to give rise to both GFP^{pos} and GFP^{neg} cells (Supplementary Fig. S1L-S1M).

Gene expression profiling reveals a dynamic metastatic state

To uncover pro-metastatic programs within the highly metastatic GFP^{pos} PDAC cell state, we performed RNA-Seq-based gene expression profiling on six pairs of GFP^{neg} and GFP^{pos} cells (Fig. 2A and Supplementary Fig. S2A-S2B). Global clustering of all samples did not clearly separate GFP^{pos} from GFP^{neg} samples (Fig. 2B). However, direct pairwise comparison of GFP^{neg} and GFP^{pos} cells uncovered hundreds of genes with consistent and significant differences (Fig. 2C-2D). Neither canonical epithelial markers nor genes related to EMT were consistently different between GFP^{neg} and GFP^{pos} cells (data not shown). We also did not observe enrichment for previously described gene expression signatures of PDAC metastasis or putative cancer stem cells in GFP^{pos} cells (13,14) (data not shown). Using flow cytometry, we confirmed that both GFP^{neg} and GFP^{pos} cancer cells had heterogeneous expression of the ductal/CSC marker CD133 and the epithelial marker EpCAM (Supplementary Fig. S2C-S2D) (33-35). Histologic features and IHC for differentiation markers confirmed that Hmga2 expression is largely independent from differentiated state (Fig. S2E).

In addition to the paired GFP^{pos} and GFP^{neg} PDAC samples, we performed RNA-Seq analyses on FACS-sorted, bulk Tom^{pos} cancer cells from primary tumors and metastases (Fig. 2A and Supplementary Fig. S2F). If metastases had stable gene expression differences from primary tumors, this approach could identify gene expression alterations that contribute to metastatic ability or growth at secondary sites. Interestingly, comparison of primary tumors to all metastases identified very few significant differentially expressed genes (Supplementary Fig. S2G). Comparisons of primary tumors to liver metastases, but not to lymph node metastases, uncover several genes that were significantly differentially expressed in the liver metastases (Supplementary Fig. S2H and S2I). Consistent with a recent report on human PDAC metastasis (36), gene set analysis uncovered a trend towards enrichment for programs related to glucose metabolism in liver metastases (Supplementary Fig. S2J). Importantly, genes that were differentially expressed between GFP^{pos} and GFP^{neg} PDAC cells were not consistently different between primary tumors and metastases, consistent with the transient nature of the GFP^{pos} cell state (Fig. 2E). Finally, high expression of a gene signature composed of genes that were more highly expressed in metastatic GFP^{pos} cancer cells predicted worse PDAC patient outcome (Fig. 2F-2G).

Identification of the transcription factor Blimp1 as a driver of metastasis

To gain further insight into the metastatic process and identify potentially pro-metastatic factors, we focused on several genes that were among the most significantly and

dramatically upregulated in GFP^{pos} cells (fold change >2; p-value <10^{-6}, Supplementary Fig. S3A). We stably knocked down five top candidate genes (*Ero1l*, *Slc16a3*, *Glut1*, *Hilpda*, and *Blimp1*) in a PDAC cell line (688M) derived from a liver metastasis from a *KPCT* mouse (Supplementary Fig. S3B-S3F). We assessed the importance of these genes in metastasis by quantifying the number of metastases that formed from subcutaneously and orthotopically transplanted tumors. These experiments suggested that the transcription factor Blimp1/Prdm1 could have pro-metastatic functions in PDAC (Supplementary Fig. S3G-S3L). Blimp1 is a transcription factor that was of particular interest due to its well-established role as a master regulator of cell fate determination during plasma B cell differentiation and primordial germ cell development (37,38). *Blimp1* was one of the most highly upregulated genes in GFP^{pos} cells, being 4- to 27-fold higher in GFP^{pos} cells (p-value < 0.05; Fig. 3A). We confirmed increased Blimp1 protein expression in sorted GFP^{pos} cells relative to GFP^{neg} cells (Fig. 3B). *Blimp1* expression was not consistently different between bulk cancer cells from primary tumors and metastases from the *KPC* mice, consistent with the unstable nature of the metastatic state (Supplementary Fig. S3M).

To further assess whether Blimp1 contributes to metastatic ability, we knocked down *Blimp1* using two independent shRNAs (688M; Supplementary Fig. S3N). *Blimp1* knockdown reduced the number of metastases seeded from subcutaneous tumors by >50-fold (p-value <0.005; Fig. 3C-3E). *Blimp1* knockdown in a second metastasis-derived PDAC cell line (1004M) also significantly reduced metastasis (Fig. 3F-3G and Supplementary Fig. S3O). Interestingly, while *Blimp1* appeared to be required for metastatic ability, overexpression of Blimp1 in multiple PDAC cell lines did not consistently enhance metastatic ability (Supplementary Fig. S3P-S3S), suggesting that expression of Blimp1 is required, but not sufficient, to drive PDAC metastasis.

Blimp1 contributes to the metastatic ability of PDAC cells in *KPC* mice

We next used a *Blimp1* conditional knockout allele to further investigate Blimp1 function in autochthonous PDAC (37). *Blimp1$^{f/f}$;Pdx1-Cre* mice were viable and their pancreata did not show obvious histological changes, suggesting that *Blimp1* is not required for pancreas development or homeostasis (data not shown). *KPCT*;*Blimp1$^{f/f}$* mice had similar overall pancreatic tumor burden but shorter survival compared to control *KPCT*;*Blimp1$^{+/+}$* mice (Supplementary Fig. S3T-S3U). Pancreata from *KPCT*;*Blimp1$^{f/f}$* mice contained PanINs as well as adenocarcinomas that were similar to PDAC in control *KPCT*;*Blimp1$^{+/+}$* mice (Supplementary Fig. S3V-S3W and data not shown). To assess the effect of *Blimp1* deficiency on metastatic progression *in vivo*, we carefully quantified the number of Tom^{pos} disseminated tumor cells (DTCs) in the peritoneal cavity as well as metastases in *KPCT*;*Blimp1$^{f/f}$* and control mice. 14 out of 15 control mice (*KPCT*;*Blimp1$^{+/+}$* and *KPCT*;*Blimp1$^{f/+}$*) developed metastases, which were often numerous and widespread in many different sites including the lymph nodes, diaphragm, lungs, and liver (Fig. 3H-3K). Conversely, only 3 out of 14 *KPCT*;*Blimp1$^{f/f}$* mice developed metastases (Fig. 3K). Additionally, peritoneal DTCs could be detected in only half of *KPCT*;*Blimp1$^{f/f}$* mice, but were present in all control mice (Fig. 3IJ-3K). Together with our observations from cell lines, these data suggest that *Blimp1* promotes metastatic proclivity of PDAC.

The highly metastatic state of PDAC is associated with a strong hypoxia signature

To place Blimp1 in a pathway involved in metastasis, we next used gene set enrichment analysis (GSEA) and gene ontology (GO) enrichment analysis to identify pathways altered in the more metastatic GFP^{pos} cells. These analyses uncovered an overwhelming enrichment for hypoxia-induced genes in GFP^{pos} cells (Fig. 4A-4D and Supplementary Table S1). Genes expressed more highly in GFP^{pos} cells were also enriched for Hif1-binding motifs near their transcription start sites and our analyses identified significant enrichments for both Hif1 and Hif2 regulated genes in GFP^{pos} cells. (Fig. 4B, Supplementary Fig. S4A-S4B, and Supplementary Table S1). Conversely, genes downregulated in GFP^{pos} cells were enriched for cell cycle processes, consistent with hypoxia-induced cell cycle arrest (Supplementary Table S1) (39). We confirmed the up-regulation of the canonical Hif1 target gene Ero1l at the protein level in sorted GFP^{pos} PDAC cells (Supplementary Fig. S4C).

Pimonidazole-defined hypoxic areas were significantly enriched for Hmga2^{pos} cells (Supplementary Fig. S4D-S4E). We also employed multicolor sequential immunoflourescence staining to show that Hmga2^{pos} areas are enriched for the expression of the canonical hypoxic target protein Glut1 (Supplementary Fig. S4F-S4G) (40).

Based on the striking enrichment of Hif targets in GFP^{pos} PDAC cells from *KPC^{colors}* mice, we also determined whether *Hmga2* expression is regulated by hypoxia. Under hypoxia, we noted only a slight increase in Hmga2 protein levels in PDAC cell lines (Supplementary Fig. S4H). While Hif target genes were enriched in Hmga2-expressing PDAC cells, *Hmga2* knockdown had no effect on the hypoxia-induced expression of canonical Hif1 target genes (Supplementary Fig. S4I). Thus, it remains unclear why Hmga2 marks this highly metastatic PDAC subpopulation but these data suggest that other aspects of the *in vivo* microenvironment either in conjunction with, or independent from, hypoxia induce Hmga2 expression in these cells.

Blimp1 is a novel hypoxia/Hif-regulated gene in human and murine PDAC

To determine whether *Blimp1* expression is regulated by hypoxia in human and murine PDAC, we assessed *Blimp1* mRNA and protein expression in PDAC cell lines exposed to hypoxia (0.5% O_2 for 24 hours). Hypoxia led to the induction of multiple canonical Hif target genes, Hif1α stabilization, and the prominent and consistent induction of *Blimp1* in two mouse and four human PDAC cell lines (Supplementary Fig. S4J-S4K and Fig. 4E-4F). Hypoxia-mediated induction of *Blimp1* in mouse and human PDAC cells was attenuated by *Hif1α* knockdown, suggesting that *Hif1α* is at least partially required for *Blimp1* induction under these conditions (Fig. 4G-4H). *BLIMP1* induction in human PDAC cell lines was also partially *HIF2* dependent (Supplementary Fig. S4B). Expression of stable HIF1α was sufficient to increase *BLIMP1* expression in PDAC cells (Fig. 4I). Finally, human PDACs with the highest *BLIMP1* expression are enriched for hypoxia signatures relative to those with the lowest *BLIMP* expression (Supplementary Fig. S4L and data not shown).

We next investigated how hypoxia and Hif induce *Blimp1* expression. To determine whether *Blimp1* can be induced indirectly by secreted factors, we measured *Blimp1* levels in PDAC cells cultured with conditioned media from hypoxia-treated cells or recombinant VEGF-A

which has been shown to induce Blimp1 in endothelial cells (41). In both cases, we did not observe robust *Blimp1* induction (Supplementary Fig. S5A-S5C). *Blimp1* was induced rapidly after exposure to hypoxia, paralleling the kinetics of canonical Hif target genes, suggesting that *Blimp1* might be induced directly by Hif (Supplementary Fig. S5D). Analysis of chromatin accessibility around the *Blimp1* locus (see below) enabled the prioritization of multiple putative distal regulatory regions that contained hypoxia-response elements (*HREs*) (Supplementary Fig. S5E). Hif1a ChIP qPCR identified a cluster of three adjacent *HREs* upstream of *Blimp1* that were bound by endogenous Hif1α in PDAC cells under hypoxia (Fig. 4J). This *HRE*-containing putative distal regulatory region conferred hypoxia responsiveness in a heterologous reporter system, which was abolished by mutation of its *HRE* motifs (Fig. 4K and Supplementary Fig. S5F-S5G). Furthermore, *Blimp1* knockdown significantly reduced the ability PDAC cells cultured under hypoxia to form spheres and had a variable effect of migratory ability in cell culture. These results suggest a role for Blimp1 in cellular behaviors related to metastatic ability (Supplementary Fig. S6A-S6I).

Blimp1 regulates a subset of hypoxic-mediated gene expression changes in PDAC

To characterize *Blimp1*'s function in hypoxic cells, we profiled the gene expression and genome-wide chromatin accessibility of sh*Control* and sh*Blimp1* PDAC cells cultured under normoxic and hypoxic conditions (Fig. 5A). Hypoxia can induce changes in chromatin state, and Blimp1 has been implicated in both plasma cell precursors and primordial germ cells as a regulator of chromatin structure (42-44). We uncovered widespread hypoxia-induced changes in chromatin accessibility, with differentially accessible regions being enriched for Hif-binding elements (Fig. 5B and Supplementary Fig. S6J-S6K). In addition, hypoxia induced genes associated with newly open chromatin regions more than those with constitutively open or close regions, suggesting that hypoxia likely regulate target gene induction in part through chromatin accessibility changes (Supplementary Fig. S6L). Interestingly, *Blimp1* knockdown had minimal impact on hypoxia-induced changes in chromatin accessibility, indicating that the function of Blimp1 is largely independent of its ability to recruit factors that lead to changes in chromatin state (Supplementary Fig. S6M-S6N).

Our parallel RNA-Seq analysis identified many genes that were dramatically and significantly altered by hypoxia (Fig. 5C-5D). As expected, canonical genes related to hypoxia were induced while cell cycle-related programs were suppressed (Fig. 5E). Consistent with the induction of *Blimp1* by hypoxia, *Blimp1* knockdown affected the expression of more genes when the cells were cultured under hypoxic conditions (Fig. 5C, Supplementary Fig. S6O, and comparison between Fig. 5F and 5G). Blimp1 was required for both the induction and repression of subsets of hypoxia-regulated genes (Supplementary Table S2). Under hypoxia, cell cycle-related programs were enriched in sh*Blimp1* cells compared to sh*Control* cells, suggesting that Blimp1 might play a role in hypoxia-induced cell cycle arrest (Fig. 5H). Approximately 12% of hypoxia-repressed genes required Blimp1 for their full suppression (N=95 of 825 hypoxia-repressed genes; Fig. 5I and Supplementary Fig. S6P-S6Q). The majority of these hypoxia-repressed, Blimp1-dependent genes were

related to cell cycle processes, consistent with the role of Blimp1 in suppressing proliferation during plasma B cell differentiation (Supplementary Fig. S6R) (45,46).

Additionally, approximately 35% of hypoxia-induced genes required Blimp1 for their full induction and were less induced under hypoxia in sh*Blimp1* cells (N=833 of 2342 hypoxia-induced genes; Fig. 5J). Genes encoding proteins involved in hypoxic responses and cell mobility were reduced in sh*Blimp1* cells compared to sh*Control* cells (Fig. 5K, Supplementary Fig. S7A-S7B, and Supplementary Table S3). We found that accessible distal regulatory regions within 500 kb of the transcription start sites of Blimp1-dependent, hypoxia-induced genes were enriched for transcription factor-binding motifs that closely resemble the Blimp1 motif (47) (*IRF1*/*IRF2*, Supplementary Fig. S7C-S7D). Although the regulation of these Blimp1-dependant genes is likely to be multifaceted, the enrichment of these motifs suggests that at least a subset of these genes may be regulated directly by Blimp1. Finally, high expression of a gene expression signature composed of hypoxia-induced, *BLIMP1*-dependent genes predicted worse PDAC patient outcome (Fig. 5L). These results suggest that *Blimp1* is a hypoxia-regulated gene that regulates a defined subset of hypoxia-controlled genes in PDAC cells.

Blimp1 is required for hypoxia-induced cell cycle repression and the induction of pro-metastatic genes

To gain additional insight into the function of Blimp1 in PDAC, we integrated our *ex vivo* RNA-Seq data from GFP^{neg} and GFP^{pos} PDAC cells with our *in vitro* RNA-Seq data from sh*Control* and sh*Blimp1* cells cultured under normoxia and hypoxia. As anticipated, a vast majority of genes that are more highly expressed in GFP^{pos} cells were also up regulated by hypoxia in PDAC cells in cell culture (Fig. 6A and Supplementary Fig. S8A-S8B). Furthermore, many hypoxia-induced genes that were more highly expressed in GFP^{pos} cells *in vivo* required *Blimp1* for optimal induction under hypoxic conditions *in vitro* (Supplementary Fig. S8A and S8C). These results underscore the strong hypoxia signature in the GFP^{pos} cells and highlight the contribution of Blimp1 to the expression of these genes.

To further relate these gene expression programs with *BLIMP1* expression in human PDAC, we used these integrated datasets to define a 36-gene signature of Blimp1-dependent, hypoxia-induced genes that are also higher in the GFP^{pos} state. Across multiple human PDAC gene expression datasets, this Blimp1 signature correlated with *BLIMP1* expression, suggesting conserved mechanism of BLIMP1 function in human PDAC *in vivo* (Fig. 6B and Supplementary Fig. S8D-S8E).

Our gene expression profiling suggested that Blimp1 might be required for hypoxia-induced cell cycle arrest. To directly test this, we cultured sh*Control* and sh*Blimp1* cells at 0.5% and 20% O_2 and assessed proliferation by short term BrdU labeling. While sh*Control* cells almost completely arrested under hypoxia, sh*Blimp1* cells continued to proliferate (Supplementary Fig. S8F-S8G). To determine whether Blimp1 reduces the proliferation of PDAC cells in tumors *in vivo*, we assessed the proliferation of cancer cells in pancreatic tumors in *KPCT*;*Blimp1*$^{f/f}$ and control *KPCT*;*Blimp1*$^{+/+}$ mice. Cancer cells in autochthonous *Blimp1*-deficient tumors had a higher mitotic index (Fig. 6C and Supplementary Fig. S8H). The higher proliferation of cancer cells in tumors from

KPCT;*Blimp1*$^{f/f}$ mice is also consistent with the shorter survival of *KPCT*;*Blimp1*$^{f/f}$ mice (Supplementary Fig. S3U).

Many of the genes that were hypoxia-induced, Blimp1-dependent, and expressed at higher levels in the more metastatic GFP^{pos} PDAC cells have been previously implicated as pro-metastatic factors in other cancer types. These genes included *Pgf*, *Dusp1*, *Hmox1*, *Car9*, *Glut1*, and *Hilpda* (48-53). Consistent with our RNA-Seq data, we observed reduced Glut1 and Car9 protein expression in PDACs in *KPCT*;*Blimp1*$^{f/f}$ mice compared to *KPCT* mice (Fig. 6D-6E and Supplementary Fig. S8H-S8M). High expression of the lipid droplet-associated protein *Hilpda* in other cancer types correlates with disease progression and metastasis (53,54). *Hildpa* expression was higher in GFP^{pos} PDAC cells, induced by hypoxia in murine and human PDAC cells, and its induction was partially *Blimp1*-dependent (Fig. 6F-6G and Supplementary Fig. S4J). *Hilpda* knockdown reduced metastasis in our initial analysis and we further confirmed that *Hilpda* knockdown in PDAC cells significantly reduced their metastatic ability (Fig. 6H-6J, Supplementary Fig. S8N, and Supplementary Fig. S5G-S5L). These data suggest that *Hilpda* is a *Blimp1*-regulated pro-metastatic factor in PDAC.

Discussion

To uncover the molecular mechanisms that drive the metastatic ability of PDAC, we initially took two unbiased gene expression-profiling approaches: analysis of Hmga2-GFP^{pos} and Hmga2-GFP^{neg} PDAC subpopulation as well as analysis of bulk cancer cells from large primary tumors and macro-metastases. In both cases, we specifically isolated cancer cells at high purity by FACS to avoid confounding our analyses with contaminating stromal cell populations. Analysis of bulk cancer cells from primary tumors and metastases uncovered few significant gene expression changes, implying that cancer cells in the largest primary tumors possess most of the molecular features required for metastatic spread.

These findings are in stark contrast to the extensive gene expression differences between large primary tumors and metastases that we uncovered in a parallel study on a Kras^{G12D}-driven, *p53*-deficient mouse model of lung adenocarcinoma (55). In the lung cancer model, large primary tumors often existed in an earlier non-metastatic state that had profound gene expression differences from metastases. In the lung, oncogenic Kras^{G12D} alone can drive extensive tumor growth and even tumors in *Kras*$^{LSL\text{-}G12D}$;*p53*$^{flox/flox}$ mice do not immediate receive benefit from being *p53* deficient (55-58). Thus, pancreatic tumors may be forced into a potentially metastatic state by the selective pressures of primary tumor growth, thereby explaining the high likelihood of metastatic spread even in patients with relatively small pancreatic tumors (59).

Despite these observations, multiple lines of evidence suggest that the metastatic ability of PDAC is still an acquired phenotype. We previously noted mice with widespread PanIN lesions that lack any disseminated tumor cells in the peritoneal cavity (60). Additionally, we and others have generated mice with clonally marked pancreatic tumors and documented that not all tumors give rise to metastases (60,61). Although we did not observe gene expression differences between large primary tumors and metastases, we have documented

microenvironment-driven metastatic heterogeneity. Our results support a model in which the development of hypoxic regions generates cells with increased metastatic ability (62). Consistent with results from autochthonous mouse models, human PDAC is a highly hypoxic cancer type (63) and the metastatic ability of orthotopically-grown, patient-derived PDAC xenografts is predicted by their level of hypoxia (64).

Hypoxia has been shown to induce metastasis in multiple cancer types through various mechanisms (reviewed in 64, 67, and 68). For example, hypoxia is related to alterations in EMT/MET, angiogenesis, local invasion and intravasation, extravasation, as well as the formation of the pre-metastatic niche (65). While some consequences of hypoxia may be relatively generalizable across cancer types, some outputs of hypoxia may also be cancer type specific, thus the importance of Blimp1 in these different steps of the metastatic cascades as well as in different cancer types remain to be determined.

Hypoxia also has a tremendous impact on the self-renewal and differentiation of the progenitor/stem cell lineages. For example, hypoxia potentiates the engraftment of human hematopoietic stem cells in recipient mice (66,67) and also helps maintain the stemness of embryonic stem and iPS cells in culture (68,69). In several cancer types, hypoxia has also been shown to play important roles in maintaining cancer stem cells (CSCs). In brain tumors, hypoxia promotes and/or maintains cancer cell stemness similar to the effect of hypoxia on *bona fide* stem cells (70,71). Several studies have identified subpopulations of murine and human PDAC cells with CSC characteristics based on their ability to generate new tumors upon transplantation (14,72). Importantly, the highly metastatic PDAC state that we identified is not directly related to previously reported CSC populations, the differentiation state of the cancer cells, or EMT. Thus, whether the highly metastatic PDAC cell state and these CSC states represent parallel or partially overlapping programs will be an important area for future study.

We initially anticipated that the high metastatic ability of Hmga2-expressing cells would be driven by Hmga2 itself. Surprisingly, this is not the case, as *Hmga2* deficiency has no impact on the metastatic ability of tumors in the *KPC* PDAC mouse model nor does it influence the induction of canonical hypoxia target genes (BMG, S-HC, MMW; manuscript in preparation and Supplementary Fig. S4I). Hmga2 could play a subtle role in the later stages of metastatic outgrowth or may simply be a marker of the metastatic state.

Mechanistically, our results uncover hypoxia-mediated induction of the transcription factor Blimp1 as one molecular link between the tumor microenvironment and transient induction of pro-metastatic gene expression programs in PDAC. Although our data show that Blimp1 can be induced through hypoxia-mediated stabilization of Hif, other factors within the tumor microenvironment may also impact Hif activity (Fig. 6L). In PDAC, Blimp1 functions as a molecular switch that promotes metastatic ability while suppressing cell division under hypoxia (Fig. 6L). Our results are consistent with the link between Blimp1 and migratory ability of human lung and breast cancer cell lines *in vitro* (73,74). *Blimp1* has not been described as a hypoxia/Hif target gene in normal cell types but hypoxia may also influence Blimp1 expression in those settings. In early embryos, where oxygen levels are low prior to the formation of major blood vessels (75), Blimp1 is expressed in primordial germ cells

where it represses somatic programs and helps maintain pluripotency (38,76). Blimp1 is also critical for the differentiation of plasma cells that are generated in secondary lymphoid organs and maintained in bone marrow, both of which have hypoxic regions (37,77,78).

In summary, our findings support the concept of microenvironmental, rather than mutational, evolution being a critical factor that fosters PDAC metastatic ability. We found that intratumoral hypoxia, which is an inevitable feature of advanced human PDAC, induces the expression of the pro-metastatic transcription factor Blimp1. The co-option of this master regulatory transcription factor is required for metastatic ability, and the molecular output of Blimp1 expression is the modulation of discrete hypoxia-induced gene expression programs. A greater understanding of the origins and molecular features of cancer cells with transient high metastatic ability could provide therapeutic opportunities to reduce metastatic spread and further our appreciation of the obligate plasticity of these cells during the metastatic process.

Methods

Mice

Kras$^{LSL\text{-}G12D}$, *p53*$^{LSL\text{-}R172R}$, *Blimp1*^{flox}, *Pdx1-Cre*, *Rosa26*$^{LSL\text{-}tdTomato}$, and *Hmga2*^{CK} mice have been described (18,20,32,37,79,80). Mice with the *Kras*$^{LSL\text{-}G12D}$ and the *R26*$^{LSL\text{-}tdTomato}$ alleles in *cis* on chromosome 6 were used to maximize retention of the *R26*$^{LSL\text{-}tdTomato}$ allele even in genomically unstable tumors. 6-10-week-old NOD/Scid/γc (NSG) mice (The Jackson Laboratory, Stock number: 005557) were used for transplantation experiments. The Stanford Institutional Animal Care and Use Committees approved all animal studies and procedures.

Histology and quantification of IHC

All histological staining were performed on paraffin-embedded, formalin-fixed sections as described previously (60). Briefly, 4 μm sections were re-hydrated and subjected to antigen retrieval before IHC was performed using Vector Lab ABC Vectastain kit. We used custom FIJI macro scripts for the quantification of IHC. See Supplemental Experimental Procedures for the detail of staining procedures and IHC quantification.

RNA-Seq data analyses

RNA and genomic DNA samples were extracted from 10^4 to 5×10^4 sorted cancer cells using Qiagen AllPrep DNA/RNA Micro Kit. RNA from *ex vivo* FACS-purified cells (15 ng/sample) were converted to cDNA and amplified with the NuGEN Ovation RNA-Seq system. Subsequently, amplified cDNA was sonicated and subjected to library preparation using the Illumina TruSeq DNA sample preparation kit. Total RNA from sh*Control* or sh*Blimp1* 688M cells cultured in 0.5% or 20% O_2 were used for the preparation of RNA-Seq libraries with Illumina's TruSeq RNA Library Prep Kit v2 according to manufacturer's protocol. Sequencing was performed on Illumina HiSeq 2000 for 100-bp paired-end (*ex vivo* samples) and non-paired-end (*in vitro* samples) reads. See Supplemental Experimental Procedures for RNA-Seq analysis details.

ATAC-Seq data analysis

Murine PDAC 688M cells cultured in 0.5% or 20% O_2 were also used for ATAC-Seq library preparation. Briefly, nuclei were extracted before incubation with TDE1 Tn5 transposase (Illumina). The fragmented genomic DNA was PCR amplified and ATAC-Seq libraries were sequenced on an Illumina NextSeq with paired-end 76bp reads using an Illumina High Output kit. ATAC-Seq data were processed as previously described with some modifications (81). See Supplemental Experimental Procedures for ATAC-Seq analysis details.

Western blotting

Cell lysates were prepared with RIPA buffer supplemented with protease inhibitors. Proteins were separated by PAGE before being transferred onto a Bio-Rad PVDF membrane. Primary antibodies were incubated in the presence of 5% skimmed milk at 4°C overnight, followed by stringent washes (3×) before staining with horseradish-peroxidase-conjugated secondary antibodies. After additional washes, enhanced chemiluminescence was performed to visualize the proteins of interest. See Supplemental Experimental Procedures for more detail of western blot analyses.

Hypoxia induction and qRT-PCR

To induce hypoxia *in vitro*, cancer cells were seeded at sub-confluency and cultured in a hypoxia chamber (Invivo2-400, Ruskin Technologies) with 0.5% O_2 for 24 hours before harvest. Cells were subsequently lysed with TRIzol (Thermo Fisher Scientific, 15596-018) directly on tissue culture dishes for RNA extraction. RNA concentration was quantified on a NanoDrop spectrophotometer (Thermo Fisher Scientific, NanoDrop 2000 UV-Vis Spectrophotometer) and converted to cDNA according to manufacturer's protocol (Thermo Fisher Scientific, 4368814). For the quantification of transcripts, SYBR green (Sigma-Aldrich, S9194) was used with specific primer pairs. *β-actin* was used as internal control. See Supplementary Data for more detailed information.

Cell lines

None of the cell lines used in this study were authenticated. The years when the PDAC cell lines were obtained are as follow: 688M, 2014; 1004M, 2014; 887M, 2017; 1814, 2015; 1810, 2015; human PDAC cell Panc1, Colo357, BxPC1, AsPC1, and Capan1 were all obtained in 2014. All PDAC cell lines that were used in experiments reported in this study were expanded early in the passage and aliquots were stored in liquid nitrogen. Thawed cells were passaged within 1-2 months for any experimental usage.

Subcutaneous transplantation of cell lines into NSG mice

688M and 1004M PDAC cells were cultured at sub-confluency shortly before harvest for transplantation. All cells used in the transplantation experiments were validated for knockdown efficacies of designated genes. Briefly, cells were trypsinized and washed 3× in cold PBS before subcutaneous injection. 2.5×10^5 cells were used per injection on the dorsal flank. The numbers of Tom^{pos} metastases in the lung were quantified by direct counting using a fluorescence dissecting scope. Alternatively, H&E sections were used to

estimate lung metastases seeded by the Tomato-negative 1004M cells. Metastases in the lung were validated by histology.

Pancreatic orthotopic transplantation

688M PDAC cell derivatives validated for efficient knockdown were washed 3× in cold PBS before resuspension in 100% Matrigel (Corning, 356231). Subsequently, a surgical procedure was performed with direct injection of the cells/Matrigel mixture into the pancreas of NSG mice. See Supplemental Experimental Procedures for more detail of the orthotopic transplantation.

Statistical analysis

For comparison between two quantitative variables, we used Student's t test when samples were not paired and paired t test for paired samples. When more than two variables were compared, both one-way ANOVA and Kruskall-Wallis test were used. For comparison of survival in Kaplan-Meier analyses, we used log-rank test for univariate survival analyses. Fisher's exact test was used in the analysis of contingency tables. Analyses were performed using Prism 6.0 (Graphpad Software Inc.).

Supplementary Material

Refer to Web version on PubMed Central for supplementary material.

Acknowledgments

We thank the Stanford Shared FACS Facility and the Protein and Nucleic Acid Facility for expert assistance; Carolyn Sinow, Santiago Naranjo, and Shashank Cheemalavugu for technical assistance; Chen-Hua Chuang and Nicholas Denko for experimental advice; Teri A Longacre for the analysis of human PDAC IHC samples; Justin A. Kenkel for help with pancreatic orthotopic transplantation procedure; Stephano Mello, Edward LaGory, and Julia Arand for reagents; Louis Leung, Chris Probert, Peyton Greenside, Andrew Seung-Hyun Koh, and Xun Lan for bioinformatics advice; Laura Attardi, Julien Sage, Jennifer Brady, Kenneth Olive, David Feldser, the Winslow laboratory, the Greenleaf laboratory, and the Stanford pancreatic cancer research community for helpful comments; and Sean Dolan and Alexandra Orantes for administrative support.

Financial Support: M.M. Winslow received a Pancreatic Cancer Action Network-AACR Award in memory of Skip Vinagh (13-20-25-WINS), Stanford Cancer Institute support grant (P30-CA124435) from the National Cancer Institute, and the award (NIH-R00CA151968) from the National Institute of Health (NIH). S. Chiou and B.M. Grüner received the Stanford Dean's Fellowship. V.I. Risca received the Walter V. and Idun Berry Fellowship. B.M. Grüner received a Pancreatic Cancer Action Network-AACR Fellowship in memory of Samuel Stroum (14-40-25-GRUE). E.E. Graves received a NIH R01 grant (CA197136). G.X. Wang received the John Merck Fund and National Institute of Mental Health R01 grant (MH099647). P. Mourrain received a NIH grant (MH09964) and the Brightfocus foundation and John Merck Fund. A.J. Giaccia received the NIH R01 grants CA67166 and CA198291.

References

1. Rahib L, Smith BD, Aizenberg R, Rosenzweig AB, Fleshman JM, Matrisian LM. Projecting cancer incidence and deaths to 2030: the unexpected burden of thyroid, liver, and pancreas cancers in the United States. Cancer research. 2014; 74(11):2913–21. [PubMed: 24840647]
2. Hidalgo M. Pancreatic cancer. The New England journal of medicine. 2010; 362(17):1605–17. [PubMed: 20427809]
3. Moskaluk CA, Hruban RH, Kern SE. p16 and K-ras gene mutations in the intraductal precursors of human pancreatic adenocarcinoma. Cancer research. 1997; 57(11):2140–3. [PubMed: 9187111]

4. Waddell N, Pajic M, Patch AM, Chang DK, Kassahn KS, Bailey P, et al. Whole genomes redefine the mutational landscape of pancreatic cancer. Nature. 2015; 518(7540):495–501. [PubMed: 25719666]
5. Wilentz RE, Iacobuzio-Donahue CA, Argani P, McCarthy DM, Parsons JL, Yeo CJ, et al. Loss of expression of Dpc4 in pancreatic intraepithelial neoplasia: Evidence that DPC4 inactivation occurs late in neoplastic progression. Cancer research. 2000; 60(7):2002–6. [PubMed: 10766191]
6. Luttges J, Galehdari H, Brocker V, Schwarte-Waldhoff I, Henne-Bruns D, Kloppel G, et al. Allelic loss is often the first hit in the biallelic inactivation of the p53 and DPC4 genes during pancreatic carcinogenesis. American Journal of Pathology. 2001; 158(5):1677–83. [PubMed: 11337365]
7. Yachida S, Jones S, Bozic I, Antal T, Leary R, Fu B, et al. Distant metastasis occurs late during the genetic evolution of pancreatic cancer. Nature. 2010; 467(7319):1114–7. [PubMed: 20981102]
8. Campbell PJ, Yachida S, Mudie LJ, Stephens PJ, Pleasance ED, Stebbings LA, et al. The patterns and dynamics of genomic instability in metastatic pancreatic cancer. Nature. 2010; 467(7319): 1109–13. [PubMed: 20981101]
9. Notta F, Chan-Seng-Yue M, Lemire M, Li YL, Wilson GW, Connor AA, et al. A renewed model of pancreatic cancer evolution based on genomic rearrangement patterns. Nature. 2016; 538(7625): 378. -+ [PubMed: 27732578]
10. Makohon-Moore AP, Zhang M, Reiter JG, Bozic I, Allen B, Kundu D, et al. Limited heterogeneity of known driver gene mutations among the metastases of individual patients with pancreatic cancer. Nature genetics. 2017; 49(3):358–66. [PubMed: 28092682]
11. Thiery JP, Acloque H, Huang RY, Nieto MA. Epithelial-mesenchymal transitions in development and disease. Cell. 2009; 139(5):871–90. [PubMed: 19945376]
12. Zheng X, Carstens JL, Kim J, Scheible M, Kaye J, Sugimoto H, et al. Epithelial-to-mesenchymal transition is dispensable for metastasis but induces chemoresistance in pancreatic cancer. Nature. 2015; 527(7579):525–30. [PubMed: 26560028]
13. Whittle MC, Izeradjene K, Rani PG, Feng L, Carlson MA, DelGiorno KE, et al. RUNX3 Controls a Metastatic Switch in Pancreatic Ductal Adenocarcinoma. Cell. 2015; 161(6):1345–60. [PubMed: 26004068]
14. Fox RG, Lytle NK, Jaquish DV, Park FD, Ito T, Bajaj J, et al. Image-based detection and targeting of therapy resistance in pancreatic adenocarcinoma. Nature. 2016; 534(7607):407–11. [PubMed: 27281208]
15. Hermann PC, Huber SL, Herrler T, Aicher A, Ellwart JW, Guba M, et al. Distinct populations of cancer stem cells determine tumor growth and metastatic activity in human pancreatic cancer. Cell stem cell. 2007; 1(3):313–23. [PubMed: 18371365]
16. Quail DF, Joyce JA. Microenvironmental regulation of tumor progression and metastasis. Nature medicine. 2013; 19(11):1423–37.
17. Feig C, Gopinathan A, Neesse A, Chan DS, Cook N, Tuveson DA. The Pancreas Cancer Microenvironment. Clinical Cancer Research. 2012; 18(16):4266–76. [PubMed: 22896693]
18. Hingorani SR, Petricoin EF, Maitra A, Rajapakse V, King C, Jacobetz MA, et al. Preinvasive and invasive ductal pancreatic cancer and its early detection in the mouse. Cancer cell. 2003; 4(6):437–50. [PubMed: 14706336]
19. Hingorani SR, Wang L, Multani AS, Combs C, Deramaudt TB, Hruban RH, et al. Trp53R172H and KrasG12D cooperate to promote chromosomal instability and widely metastatic pancreatic ductal adenocarcinoma in mice. Cancer cell. 2005; 7(5):469–83. [PubMed: 15894267]
20. Chiou SH, Kim-Kiselak C, Risca VI, Heimann MK, Chuang CH, Burds AA, et al. A conditional system to specifically link disruption of protein-coding function with reporter expression in mice. Cell reports. 2014; 7(6):2078–86. [PubMed: 24931605]
21. Bardeesy N, Cheng KH, Berger JH, Chu GC, Pahler J, Olson P, et al. Smad4 is dispensable for normal pancreas development yet critical in progression and tumor biology of pancreas cancer. Genes & development. 2006; 20(22):3130–46. [PubMed: 17114584]
22. Aguirre AJ, Bardeesy N, Sinha M, Lopez L, Tuveson DA, Horner J, et al. Activated Kras and Ink4a/Arf deficiency cooperate to produce metastatic pancreatic ductal adenocarcinoma. Genes & development. 2003; 17(24):3112–26. DOI: 10.1101/gad.1158703 [PubMed: 14681207]

23. Bardeesy N, Aguirre AJ, Chu GC, Cheng KH, Lopez LV, Hezel AF, et al. Both p16(Ink4a) and the p19(Arf)-p53 pathway constrain progression of pancreatic adenocarcinoma in the mouse. Proceedings of the National Academy of Sciences of the United States of America. 2006; 103(15): 5947–52. [PubMed: 16585505]
24. Raskin L, Fullen DR, Giordano TJ, Thomas DG, Frohm ML, Cha KB, et al. Transcriptome profiling identifies HMGA2 as a biomarker of melanoma progression and prognosis. The Journal of investigative dermatology. 2013; 133(11):2585–92. [PubMed: 23633021]
25. Hristov AC, Cope L, Reyes MD, Singh M, Iacobuzio-Donahue C, Maitra A, et al. HMGA2 protein expression correlates with lymph node metastasis and increased tumor grade in pancreatic ductal adenocarcinoma. Modern pathology : an official journal of the United States and Canadian Academy of Pathology, Inc. 2009; 22(1):43–9.
26. Meyer B, Loeschke S, Schultze A, Weigel T, Sandkamp M, Goldmann T, et al. HMGA2 overexpression in non-small cell lung cancer. Mol Carcinog. 2007; 46(7):503–11. [PubMed: 17477356]
27. Motoyama K, Inoue H, Nakamura Y, Uetake H, Sugihara K, Mori M. Clinical significance of high mobility group A2 in human gastric cancer and its relationship to let-7 microRNA family. Clinical cancer research : an official journal of the American Association for Cancer Research. 2008; 14(8):2334–40. [PubMed: 18413822]
28. Piscuoglio S, Zlobec I, Pallante P, Sepe R, Esposito F, Zimmermann A, et al. HMGA1 and HMGA2 protein expression correlates with advanced tumour grade and lymph node metastasis in pancreatic adenocarcinoma. Histopathology. 2012; 60(3):397–404. [PubMed: 22276603]
29. Sun M, Song CX, Huang H, Frankenberger CA, Sankarasharma D, Gomes S, et al. HMGA2/TET1/HOXA9 signaling pathway regulates breast cancer growth and metastasis. Proceedings of the National Academy of Sciences of the United States of America. 2013; 110(24):9920–5. [PubMed: 23716660]
30. Wang X, Liu X, Li AY, Chen L, Lai L, Lin HH, et al. Overexpression of HMGA2 promotes metastasis and impacts survival of colorectal cancers. Clinical cancer research : an official journal of the American Association for Cancer Research. 2011; 17(8):2570–80. [PubMed: 21252160]
31. Abe N, Watanabe T, Suzuki Y, Matsumoto N, Masaki T, Mori T, et al. An increased high-mobility group A2 expression level is associated with malignant phenotype in pancreatic exocrine tissue. Br J Cancer. 2003; 89(11):2104–9. [PubMed: 14647145]
32. Madisen L, Zwingman TA, Sunkin SM, Oh SW, Zariwala HA, Gu H, et al. A robust and high-throughput Cre reporting and characterization system for the whole mouse brain. Nature neuroscience. 2010; 13(1):133–40. [PubMed: 20023653]
33. Banerjee S, Nomura A, Sangwan V, Chugh R, Dudeja V, Vickers SM, et al. CD133+ tumor initiating cells in a syngenic murine model of pancreatic cancer respond to Minnelide. Clinical cancer research : an official journal of the American Association for Cancer Research. 2014; 20(9):2388–99. [PubMed: 24634377]
34. Lee CJ, Dosch J, Simeone DM. Pancreatic cancer stem cells. Journal of clinical oncology : official journal of the American Society of Clinical Oncology. 2008; 26(17):2806–12. [PubMed: 18539958]
35. Viale A, Pettazzoni P, Lyssiotis CA, Ying H, Sanchez N, Marchesini M, et al. Oncogene ablation-resistant pancreatic cancer cells depend on mitochondrial function. Nature. 2014; 514(7524):628–32. [PubMed: 25119024]
36. McDonald OG, Li X, Saunders T, Tryggvadottir R, Mentch SJ, Warmoes MO, et al. Epigenomic reprogramming during pancreatic cancer progression links anabolic glucose metabolism to distant metastasis. Nature genetics. 2017; 49(3):367–76. [PubMed: 28092686]
37. Shapiro-Shelef M, Lin KI, McHeyzer-Williams LJ, Liao J, McHeyzer-Williams MG, Calame K. Blimp-1 is required for the formation of immunoglobulin secreting plasma cells and pre-plasma memory B cells. Immunity. 2003; 19(4):607–20. [PubMed: 14563324]
38. Ohinata Y, Payer B, O'Carroll D, Ancelin K, Ono Y, Sano M, et al. Blimp1 is a critical determinant of the germ cell lineage in mice. Nature. 2005; 436(7048):207–13. [PubMed: 15937476]

39. Gardner LB, Li Q, Park MS, Flanagan WM, Semenza GL, Dang CV. Hypoxia inhibits G1/S transition through regulation of p27 expression. The Journal of biological chemistry. 2001; 276(11):7919–26. [PubMed: 11112789]
40. Micheva KD, Smith SJ. Array tomography: a new tool for imaging the molecular architecture and ultrastructure of neural circuits. Neuron. 2007; 55(1):25–36. [PubMed: 17610815]
41. Arulanandam R, Batenchuk C, Angarita FA, Ottolino-Perry K, Cousineau S, Mottashed A, et al. VEGF-Mediated Induction of PRD1-BF1/Blimp1 Expression Sensitizes Tumor Vasculature to Oncolytic Virus Infection. Cancer cell. 2015; 28(2):210–24. [PubMed: 26212250]
42. Melvin A, Rocha S. Chromatin as an oxygen sensor and active player in the hypoxia response. Cell Signal. 2012; 24(1):35–43. [PubMed: 21924352]
43. Ancelin K, Lange UC, Hajkova P, Schneider R, Bannister AJ, Kouzarides T, et al. Blimp1 associates with Prmt5 and directs histone arginine methylation in mouse germ cells. Nature cell biology. 2006; 8(6):623–30. [PubMed: 16699504]
44. Minnich M, Tagoh H, Bonelt P, Axelsson E, Fischer M, Cebolla B, et al. Multifunctional role of the transcription factor Blimp-1 in coordinating plasma cell differentiation. Nature immunology. 2016; 17(3):331–43. [PubMed: 26779602]
45. Lin Y, Wong K, Calame K. Repression of c-myc transcription by Blimp-1, an inducer of terminal B cell differentiation. Science. 1997; 276(5312):596–9. [PubMed: 9110979]
46. Shaffer AL, Lin KI, Kuo TC, Yu X, Hurt EM, Rosenwald A, et al. Blimp-1 orchestrates plasma cell differentiation by extinguishing the mature B cell gene expression program. Immunity. 2002; 17(1):51–62. [PubMed: 12150891]
47. Kuo TC, Calame KL. B lymphocyte-induced maturation protein (Blimp)-1, IFN regulatory factor (IRF)-1, and IRF-2 can bind to the same regulatory sites. Journal of immunology. 2004; 173(9): 5556–63.
48. Lou Y, McDonald PC, Oloumi A, Chia S, Ostlund C, Ahmadi A, et al. Targeting tumor hypoxia: suppression of breast tumor growth and metastasis by novel carbonic anhydrase IX inhibitors. Cancer research. 2011; 71(9):3364–76. [PubMed: 21415165]
49. Kawamura T, Kusakabe T, Sugino T, Watanabe K, Fukuda T, Nashimoto A, et al. Expression of glucose transporter-1 in human gastric carcinoma: association with tumor aggressiveness, metastasis, and patient survival. Cancer. 2001; 92(3):634–41. [PubMed: 11505409]
50. Chaturvedi P, Gilkes DM, Wong CC, Kshitiz, Luo W, Zhang H, et al. Hypoxia-inducible factor-dependent breast cancer-mesenchymal stem cell bidirectional signaling promotes metastasis. The Journal of clinical investigation. 2013; 123(1):189–205. [PubMed: 23318994]
51. Moncho-Amor V, Ibanez de Caceres I, Bandres E, Martinez-Poveda B, Orgaz JL, Sanchez-Perez I, et al. DUSP1/MKP1 promotes angiogenesis, invasion and metastasis in non-small-cell lung cancer. Oncogene. 2011; 30(6):668–78. [PubMed: 20890299]
52. Dey S, Sayers CM, Verginadis II, Lehman SL, Cheng Y, Cerniglia GJ, et al. ATF4-dependent induction of heme oxygenase 1 prevents anoikis and promotes metastasis. The Journal of clinical investigation. 2015; 125(7):2592–608. [PubMed: 26011642]
53. Seo T, Konda R, Sugimura J, Iwasaki K, Nakamura Y, Fujioka T. Expression of hypoxia-inducible protein 2 in renal cell carcinoma: A promising candidate for molecular targeting therapy. Oncology letters. 2010; 1(4):697–701. [PubMed: 22966366]
54. Kim SH, Wang D, Park YY, Katoh H, Margalit O, Sheffer M, et al. HIG2 promotes colorectal cancer progression via hypoxia-dependent and independent pathways. Cancer letters. 2013; 341(2):159–65. [PubMed: 23916472]
55. Chuang CH, Greenside P, Rogers Z, Brady J, Yang D, Caswell D, et al. Molecular definition of a metastatic lung cancer state reveals a targetable CD109/Jak/Stat axis. Nature medicine. 2017 in press.
56. Feldser DM, Kostova KK, Winslow MM, Taylor SE, Cashman C, Whittaker CA, et al. Stage-specific sensitivity to p53 restoration during lung cancer progression. Nature. 2010; 468(7323): 572–5. [PubMed: 21107428]
57. Muzumdar MD, Dorans KJ, Chung KM, Robbins R, Tammela T, Gocheva V, et al. Clonal dynamics following p53 loss of heterozygosity in Kras-driven cancers. Nature communications. 2016; 7:12685.

58. Rogers ZN, McFarland CD, Winters IP, Naranjo S, Chuang CH, Petrov D, et al. A quantitative and multiplexed approach to uncover the fitness landscape of tumor suppression in vivo. Nature methods. 2017
59. Fortner JG, Klimstra DS, Senie RT, Maclean BJ. Tumor size is the primary prognosticator for pancreatic cancer after regional pancreatectomy. Annals of surgery. 1996; 223(2):147–53. [PubMed: 8597508]
60. Chiou SH, Winters IP, Wang J, Naranjo S, Dudgeon C, Tamburini FB, et al. Pancreatic cancer modeling using retrograde viral vector delivery and in vivo CRISPR/Cas9-mediated somatic genome editing. Genes & development. 2015; 29(14):1576–85. [PubMed: 26178787]
61. Maddipati R, Stanger BZ. Pancreatic Cancer Metastases Harbor Evidence of Polyclonality. Cancer discovery. 2015; 5(10):1086–97. [PubMed: 26209539]
62. Bertout JA, Patel SA, Simon MC. The impact of O2 availability on human cancer. Nature reviews Cancer. 2008; 8(12):967–75. [PubMed: 18987634]
63. Koong AC, Mehta VK, Le QT, Fisher GA, Terris DJ, Brown JM, et al. Pancreatic tumors show high levels of hypoxia. International journal of radiation oncology, biology, physics. 2000; 48(4): 919–22.
64. Chang Q, Jurisica I, Do T, Hedley DW. Hypoxia predicts aggressive growth and spontaneous metastasis formation from orthotopically grown primary xenografts of human pancreatic cancer. Cancer research. 2011; 71(8):3110–20. [PubMed: 21343390]
65. Gilkes DM, Semenza GL. Role of hypoxia-inducible factors in breast cancer metastasis. Future oncology. 2013; 9(11):1623–36. [PubMed: 24156323]
66. Danet GH, Pan Y, Luongo JL, Bonnet DA, Simon MC. Expansion of human SCID-repopulating cells under hypoxic conditions. The Journal of clinical investigation. 2003; 112(1):126–35. [PubMed: 12840067]
67. Cipolleschi MG, Dello Sbarba P, Olivotto M. The role of hypoxia in the maintenance of hematopoietic stem cells. Blood. 1993; 82(7):2031–7. [PubMed: 8104535]
68. Ezashi T, Das P, Roberts RM. Low O2 tensions and the prevention of differentiation of hES cells. Proceedings of the National Academy of Sciences of the United States of America. 2005; 102(13): 4783–8. [PubMed: 15772165]
69. Yoshida Y, Takahashi K, Okita K, Ichisaka T, Yamanaka S. Hypoxia enhances the generation of induced pluripotent stem cells. Cell stem cell. 2009; 5(3):237–41. [PubMed: 19716359]
70. Soeda A, Park M, Lee D, Mintz A, Androutsellis-Theotokis A, McKay RD, et al. Hypoxia promotes expansion of the CD133-positive glioma stem cells through activation of HIF-1alpha. Oncogene. 2009; 28(45):3949–59. [PubMed: 19718046]
71. Heddleston JM, Li Z, McLendon RE, Hjelmeland AB, Rich JN. The hypoxic microenvironment maintains glioblastoma stem cells and promotes reprogramming towards a cancer stem cell phenotype. Cell cycle. 2009; 8(20):3274–84. [PubMed: 19770585]
72. Ishizawa K, Rasheed ZA, Karisch R, Wang QJ, Kowalski J, Susky E, et al. Tumor-Initiating Cells Are Rare in Many Human Tumors. Cell stem cell. 2010; 7(3):279–82. [PubMed: 20804964]
73. Romagnoli M, Belguise K, Yu Z, Wang X, Landesman-Bollag E, Seldin DC, et al. Epithelial-to-mesenchymal transition induced by TGF-beta1 is mediated by Blimp-1-dependent repression of BMP-5. Cancer research. 2012; 72(23):6268–78. [PubMed: 23054396]
74. Yu Z, Sato S, Trackman PC, Kirsch KH, Sonenshein GE. Blimp1 activation by AP-1 in human lung cancer cells promotes a migratory phenotype and is inhibited by the lysyl oxidase propeptide. PloS one. 2012; 7(3):e33287. [PubMed: 22438909]
75. Walls JR, Coultas L, Rossant J, Henkelman RM. Three-dimensional analysis of vascular development in the mouse embryo. PloS one. 2008; 3(8):e2853. [PubMed: 18682734]
76. Vincent SD, Dunn NR, Sciammas R, Shapiro-Shalef M, Davis MM, Calame K, et al. The zinc finger transcriptional repressor Blimp1/Prdm1 is dispensable for early axis formation but is required for specification of primordial germ cells in the mouse. Development. 2005; 132(6): 1315–25. [PubMed: 15750184]
77. Caldwell CC, Kojima H, Lukashev D, Armstrong J, Farber M, Apasov SG, et al. Differential effects of physiologically relevant hypoxic conditions on T lymphocyte development and effector functions. Journal of immunology. 2001; 167(11):6140–9.

78. Cho SH, Raybuck AL, Stengel K, Wei M, Beck TC, Volanakis E, et al. Germinal centre hypoxia and regulation of antibody qualities by a hypoxia response system. Nature. 2016; 537(7619):234–8. [PubMed: 27501247]

79. Jackson EL, Willis N, Mercer K, Bronson RT, Crowley D, Montoya R, et al. Analysis of lung tumor initiation and progression using conditional expression of oncogenic K-ras. Genes & development. 2001; 15(24):3243–8. [PubMed: 11751630]

80. Olive KP, Tuveson DA, Ruhe ZC, Yin B, Willis NA, Bronson RT, et al. Mutant p53 gain of function in two mouse models of Li-Fraumeni syndrome. Cell. 2004; 119(6):847–60. [PubMed: 15607980]

81. Buenrostro JD, Giresi PG, Zaba LC, Chang HY, Greenleaf WJ. Transposition of native chromatin for fast and sensitive epigenomic profiling of open chromatin, DNA-binding proteins and nucleosome position. Nature methods. 2013; 10(12):1213–8. [PubMed: 24097267]

Significance

PDAC is an almost uniformly lethal cancer, largely due to its tendency for metastasis. We define a highly metastatic subpopulation of cancer cells, uncover a key transcriptional regulator of metastatic ability, and define hypoxia as an important factor within the tumor microenvironment that increases the metastatic proclivity.

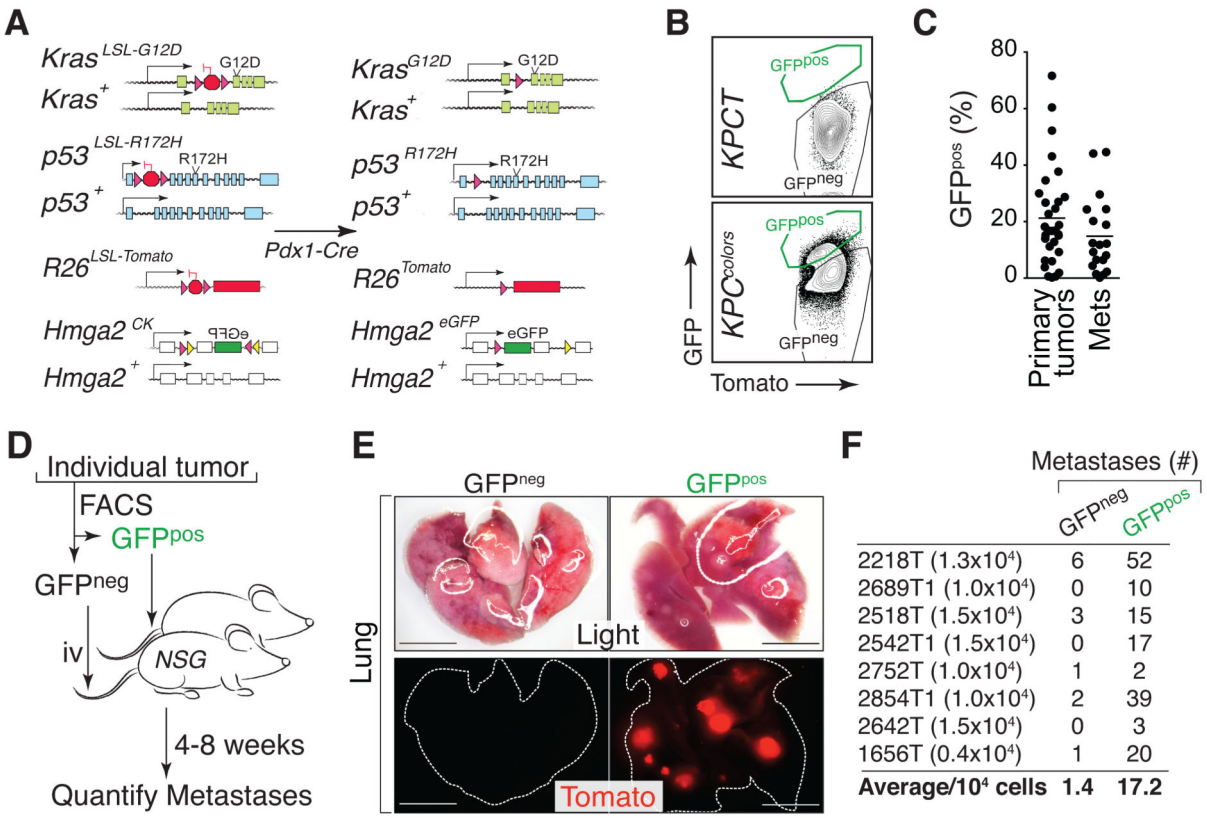

Figure 1. Identification of a subpopulation of highly metastatic pancreatic cancer cells

(A) Alleles in the *KPC*^{colors} model (*Kras*$^{LSL\text{-}G12D/+}$;*p53*$^{LSL\text{-}R172H/+}$;*Hmga2*$^{CK/+}$;*R26*$^{LSL\text{-}Tom}$;*Pdx1-Cre*) before and after Cre-mediated recombination.

(B) Representative FACS plots of dissociated pancreatic cancer cells from *Kras*$^{LSL\text{-}G12D/+}$;*p53*$^{LSL\text{-}R172H/+}$;*Pdx1-Cre*;*R26*$^{LSL\text{-}Tom}$ (*KPCT*) and *KPC*^{colors} mice. FSC/SSC-gated lineage^{neg} (CD45^{neg}CD31^{neg}F4/80^{neg}Ter119^{neg}) viable (DAPI^{neg}) Tomato^{pos} cells are shown.

(C) Individual primary tumors and metastases (Mets) have variable proportions of GFP^{pos} cells. Each dot is a tumor and the bar is the mean.

(D) Metastatic ability of GFP^{neg} and GFP^{pos} subpopulations from individual tumors was assessed by intravenous (*i.v.*) transplantation into recipient mice.

(E) Light and fluorescent dissecting scope images of lungs from recipient mice after *i.v.* transplantation of GFP^{neg} or GFP^{pos} PDAC cells from an individual tumor from a *KPC*^{colors} mouse. Scale bars = 0.5 cm.

(F) Number of cells injected and the number of metastases is indicated for each matched pair. The average number of metastases per 10^4 GFP^{neg} and GFP^{pos} PDAC cells is shown. p-value < 0.008 by Wilcoxon matched-pair signed rank test.

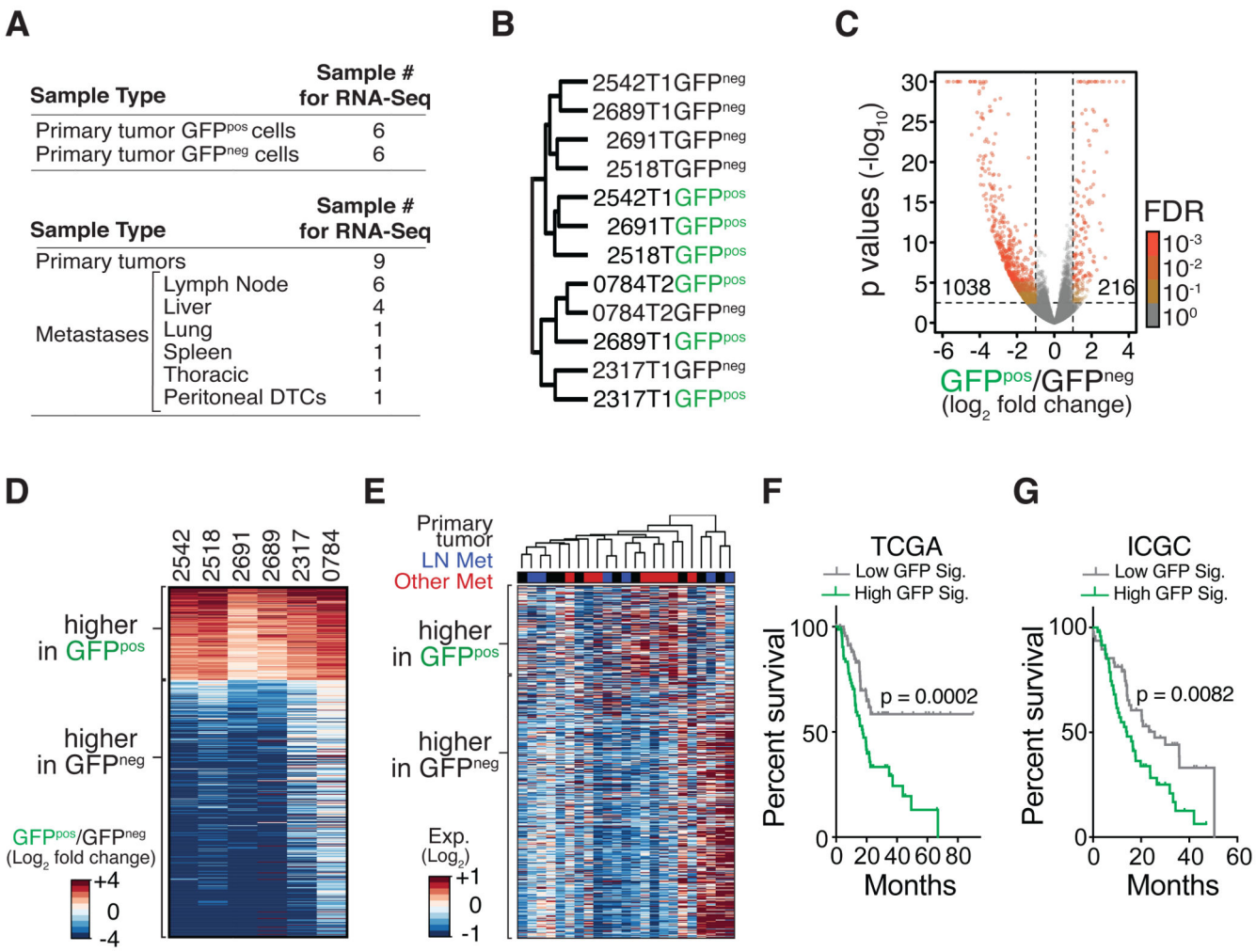

Figure 2. Highly metastatic PDAC cells have a unique gene signature, which is not preserved in metastases but predicts poor patient outcome

(A) Samples used for gene expression profiling.

(B) Consensus clustering of GFP^{neg} and GFP^{pos} PDAC cell populations using Spearman correlation.

(C) Comparison of the gene expression in GFP^{neg} and GFP^{pos} cells. Number of genes with absolute $\log_2$ fold change > 1 and adjusted p-value < 0.05 (adjusted with maximum false discovery rate (FDR) of 0.1) is shown.

(D) Heatmap of genes differentially expressed between GFP^{neg} and GFP^{pos} PDAC cells, defined by paired comparison between GFP^{neg} and GFP^{pos} cells with a p-value < 0.05, false discovery rate < or = 0.001, and absolute $\log_2$ fold change > 1.

(E) Heatmap of the expression of differentially expressed genes between GFP^{neg} and GFP^{pos} PDAC cells in bulk cancer cells from primary tumors and metastases from *KPCT* mice.

(F, G) A gene expression signature based on genes that are more highly expressed in GFP^{pos} cells (GFP Sig.) predicts shorter PDAC patient survival. PDAC patients from The Cancer Genome Atlas (F) and the International Cancer Genome Consortium (G) were split into top

and bottom 50% (High GFP Sig. and Low GFP Sig., respectively) based on the single sample GSEA scores for GFP signature genes. p-values were calculated by log-rank test.

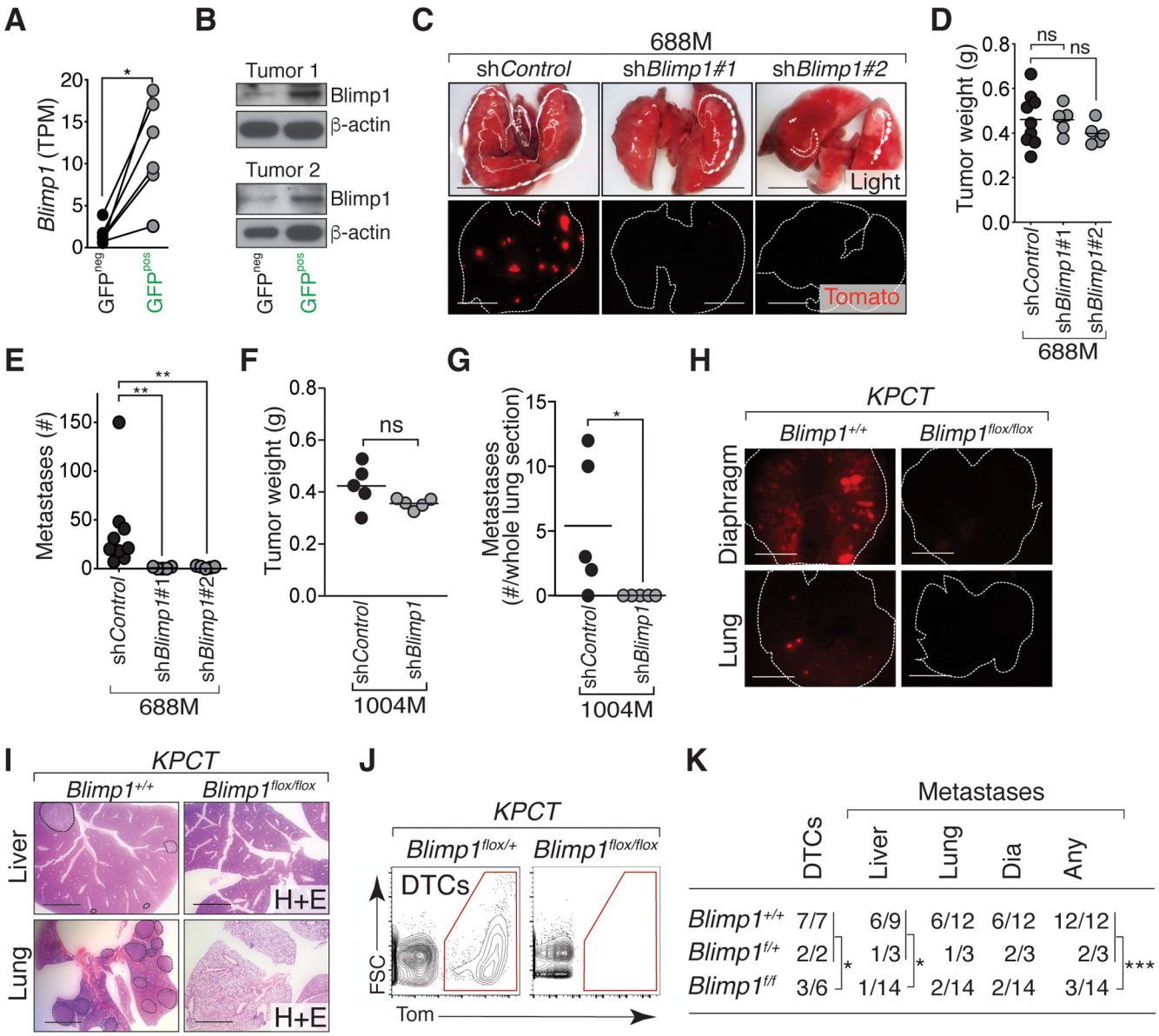

Figure 3. Highly metastatic PDAC cells express Blimp1, which is required for PDAC metastatic ability

(A) Expression of *Blimp1* (transcripts per million, TPM) in GFP^{pos} and GFP^{neg} cells (*, p-value < 0.05 by paired t test).

(B) Blimp1 protein expression in GFP^{pos} and GFP^{neg} PDAC cells from two *KPC^{colors}* tumors. Blimp1 size is estimated ~60kD.

(C) Representative dissecting scope images of lung metastases in mice with subcutaneous tumors from 688M cells with *Control* or *Blimp1* knockdown. Scale bars = 0.5 cm.

(D) Subcutaneous tumor growth of sh*Control* and sh*Blimp1* PDAC cell line derivatives (688M). Each dot represents the average weight (g) of all tumors from a mouse and the bar is the average. In these experiments, mice were purposefully sacrificed when the

subcutaneous tumors reached a designated size (Supplementary Methods). ns, not statistically significant by Student's t test.

(E) Quantification of lung metastases in mice with subcutaneous tumors. Each dot represents a mouse and the bar is the mean. Data represent pooled results from 2 experiments. **, p-value < 0.005 by Student's t test.

(F) Subcutaneous tumor growth of sh*Control* and sh*Blimp1* PDAC cell line derivatives (1004M). Each dot represents the average weight (g) of all tumors from a mouse and the bar is the average. In these experiments, mice were purposefully sacrificed when the subcutaneous tumors reached a designated size (Supplementary Methods). ns, not statistically significant by Student's t test.

(G) Quantification of lung metastases in mice with subcutaneous tumors. Each dot represents a mouse and the bar is the mean. Data represent pooled results from 2 experiments. *, p-value < 0.05 by Student's t test.

(H) Representative images of lung and diaphragm metastases in *KPTC*;*Blimp1*$^{+/+}$ and *KPCT*;*Blimp1*$^{flox/flox}$ mice. Scale bars = 0.5 cm. Lung and diaphragm are outlined with dotted white line.

(I) *KPCT*;*Blimp1*$^{flox/flox}$ mice have fewer metastases. Representative H&E stained sections of lung and liver metastases in *KPTC*;*Blimp1*$^{+/+}$ and *KPCT*;*Blimp1*$^{flox/flox}$ mice. Scale bars = 0.5 cm. Organs with Tomato^{pos} metastases are outlined.

(J) *KPCT*;*Blimp1*$^{flox/flox}$ mice have fewer disseminated tumor cells (DTCs). Representative FACS plots of viable, lineage^{neg}Tomato^{pos} cancer cells in the peritoneal cavity of control *KPCT*;*Blimp1*$^{flox/+}$ and *KPCT*;*Blimp1*$^{flox/flox}$ mice are shown. gated on lineage^{neg} single cells.

(K) Number of mice with DTCs and metastases. *, p-value < 0.05; ***, p-value < 0.0005 by Fisher's exact test. Dia, diaphragm. p-values for other comparisons between control (*KPTC*;*Blimp1*$^{+/+}$ and *KPCT*;*Blimp1*$^{flox/+}$) mice and *KPCT*;*Blimp1*$^{flox/flox}$ mice are: lung, 0.1086 and Dia, 0.0502.

A

Gene Set (All curated)	NES	NOM p-value	FWER p-value
QI_HYPOXIA	3.34	0	0
GROSS_HYPOXIA_VIA_ELK3/HIF1A_UP	3.23	0	0
LEONARD_HYPOXIA	3.04	0	0
FARDIN_HYPOXIA_11	3.02	0	0
GROSS_HYPOXIA_VIA_HIF1A_DN	3.01	0	0
ELVIDGE_HYPOXIA_UP	3.00	0	0

10 of the next 11 are hypoxia or Hif-related programs

B

Gene Set (All motif)	NES	NOM p-value	FWER p-value
HIF1_Q5	2.02	0	0

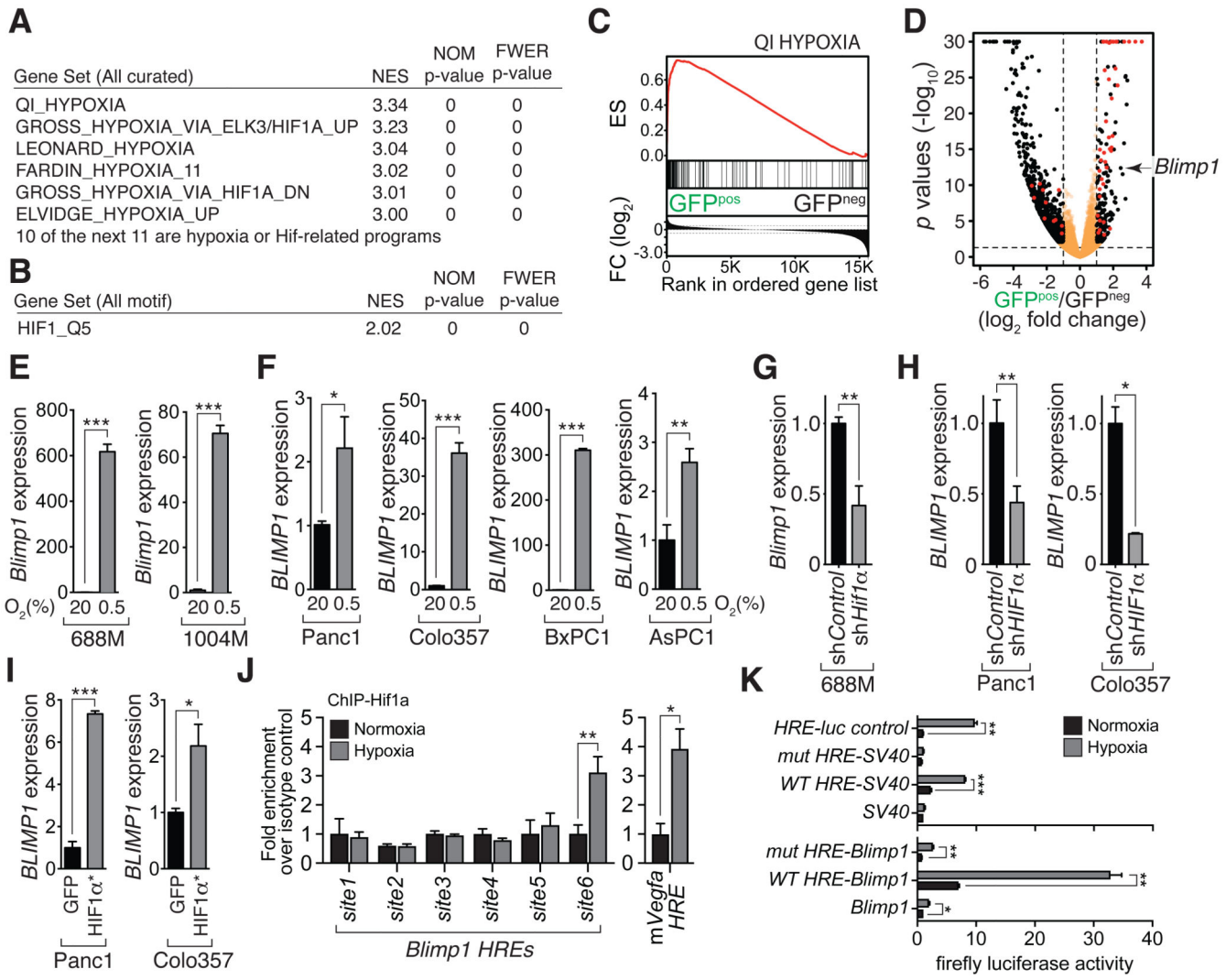

Figure 4. Blimp1 is regulated by hypoxia/Hif1 in murine and human pancreatic cancer cells

(A) The GFP^{pos} PDAC cell state is enriched for hypoxia-induced genes and Hif-targets.

(B) Enrichment for the Hif1-binding site in the promoters of genes up-regulated in the GFP^{pos} cell state.

(C) Significant enrichment for hypoxia-regulated genes in GFP^{pos} cells. ES, enrichment score; FC, fold change.

(D) Volcano plot of the gene expression differences between GFP^{pos} and GFP^{neg} cancer cell populations. Fold change and adjusted p-values were generated by taking paired samples into consideration. Red dots denote annotated Hif1 target genes.

(E,F) Hypoxia (0.5% O_2 for 24 hours) induces *Blimp1* expression in two mouse PDAC cell lines (E) and four human PDAC cell lines (F). *, p-value < 0.05; **, p-value < 0.005; ***, p-value < 0.0005 by Student's t test. Mean +/- SD of triplicate wells in shown.

(G,H) Knockdown of *Hif1a* in the murine 688M cells (G) and *HIF1a* in two human PDAC cell lines (H) reduces hypoxia-induced *Blimp1* and *BLIMP1* upregulation, respectively.

Mean +/- SD of triplicate wells in shown. *, p-value < 0.05; **, p-value < 0.005 by Student's t test.

(I) Expression of stabilized HIF1α increases *BLIMP1* expression in two human PDAC cell lines. *, p-value < 0.05; **, p-value < 0.0005 by Student's t test. Mean +/- SD of triplicate wells in shown.

(J) Chromatin immunoprecipitation (ChIP) qPCR-quantified Hif1α binding at an *HRE*-containing region 240 kb upstream of the *Blimp1* TSS (*site6*). 688M cells were cultured under normoxia or hypoxia before ChIP. Six *HRE* were quantified for enrichment of Hif1a binding by qPCR. An *HRE* region in the *Vegfa* locus is a positive control for hypoxia-induced Hif1α binding. *, p-value < 0.05; **, p-value < 0.005 by Student's t test.

(K) The wildtype *site6* (*WT-HRE*), but not *site6* with all three *HREs* mutated (*mut-HRE*), conferred hypoxia responsiveness on a *SV40* promoter or a 1.6kb *Blimp1* promoter. Representative results of 688M cells transfected with indicated reporters cultured under normoxia or hypoxia. Means +/- SD of triplicated ratios of firefly luciferase normalized to co-transfected Renilla luciferase reporter are shown.

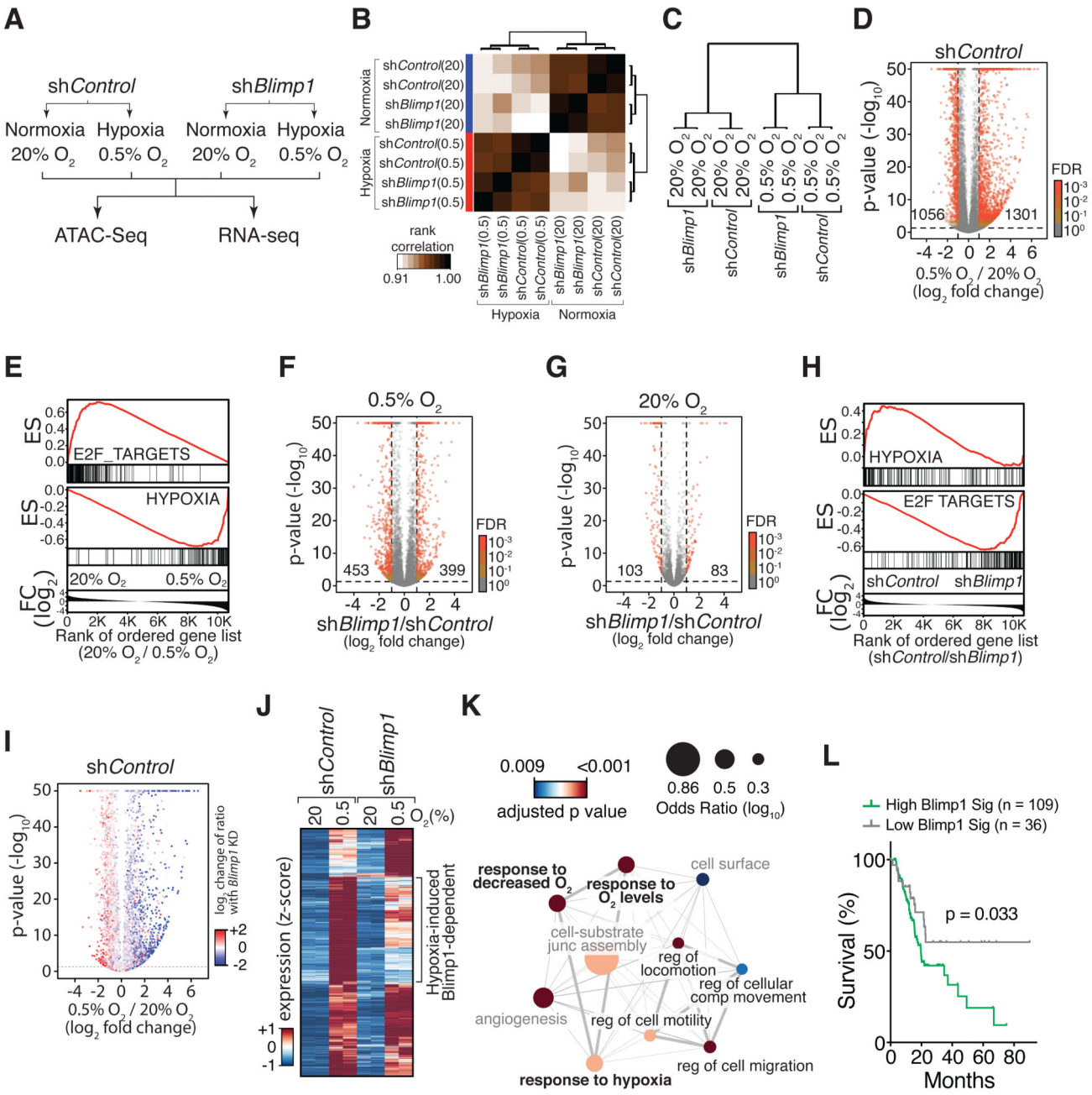

Figure 5. Blimp1 regulates the expression of a subset of hypoxia-induced genes

(A) The PDAC cell line 688M was cultured for 24 hours under normoxia/hypoxia *in vitro* for RNA-Seq and ATAC-Seq analyses.

(B) Pearson correlation of all samples based on global chromatin accessibility determined from ATAC-Seq analysis.

(C) Clustering of correlation of samples based on the global gene expression derived from RNA-Seq analysis.

(D) Hypoxia-induced changes in gene expression. Numbers of differentially expressed genes that are significant with FDR < 0.001 are shown.

(E) Genes suppressed by hypoxia are significantly enriched for cell cycle-related programs (E2F_TARGETS). Genes induced by hypoxia are significantly enriched for a hypoxia signature. ES, enrichment score; FC, fold change.

(F,G) Gene expression differences between sh*Blimp1* and sh*Control* cells cultured under hypoxia (F) and normoxia (G). Numbers of differentially expressed genes that are significant with FDR < 0.001 are shown.

(H) Blimp1-repressed genes under hypoxia are significantly enriched for cell cycle-related programs (bottom panel). GSEA was conducted by comparing the transcriptomes of sh*Control* and sh*Blimp1* cells cultured under hypoxia. ES, enrichment score; FC, fold change.

(I) *Blimp1* knockdown reduces the induction of hypoxia-induced genes (blue) while de-represses hypoxia-suppressed genes (red). Change of ratio under *Blimp1* knockdown is defined as the ratio of a, “fold change of gene expression induced by hypoxia in sh*Blimp1* cells” over b, “fold change of gene expression induced by hypoxia in sh*Control* cells”. p-values are adjusted with a FDR = 0.1.

(J) About 35% of hypoxia-induced genes required Blimp1 for their full induction and were less induced by hypoxia in sh*Blimp1* cells ($\log_2$ fold change < -0.5).

(K) GO term analysis of hypoxia-induced, Blimp1-dependent genes defined in (J). Significantly enriched biological processes are shown. Node size represents odds ratio ($\log_{10}$) and color shows adjusted p-values. Thickness of lines connecting nodes represents percent of shared genes between connected processes. Hypoxia (bold) and cell mobility (black font) related processes are highlighted.

(L) Hypoxia-induced, Blimp1-dependent genes (BLIMP1 Sig.) predict PDAC patient outcome. Single sample GSEA (ssGSEA) scores for the BLIMP1 Sig. were used to separate the top three from the bottom quartile of TCGA patients.

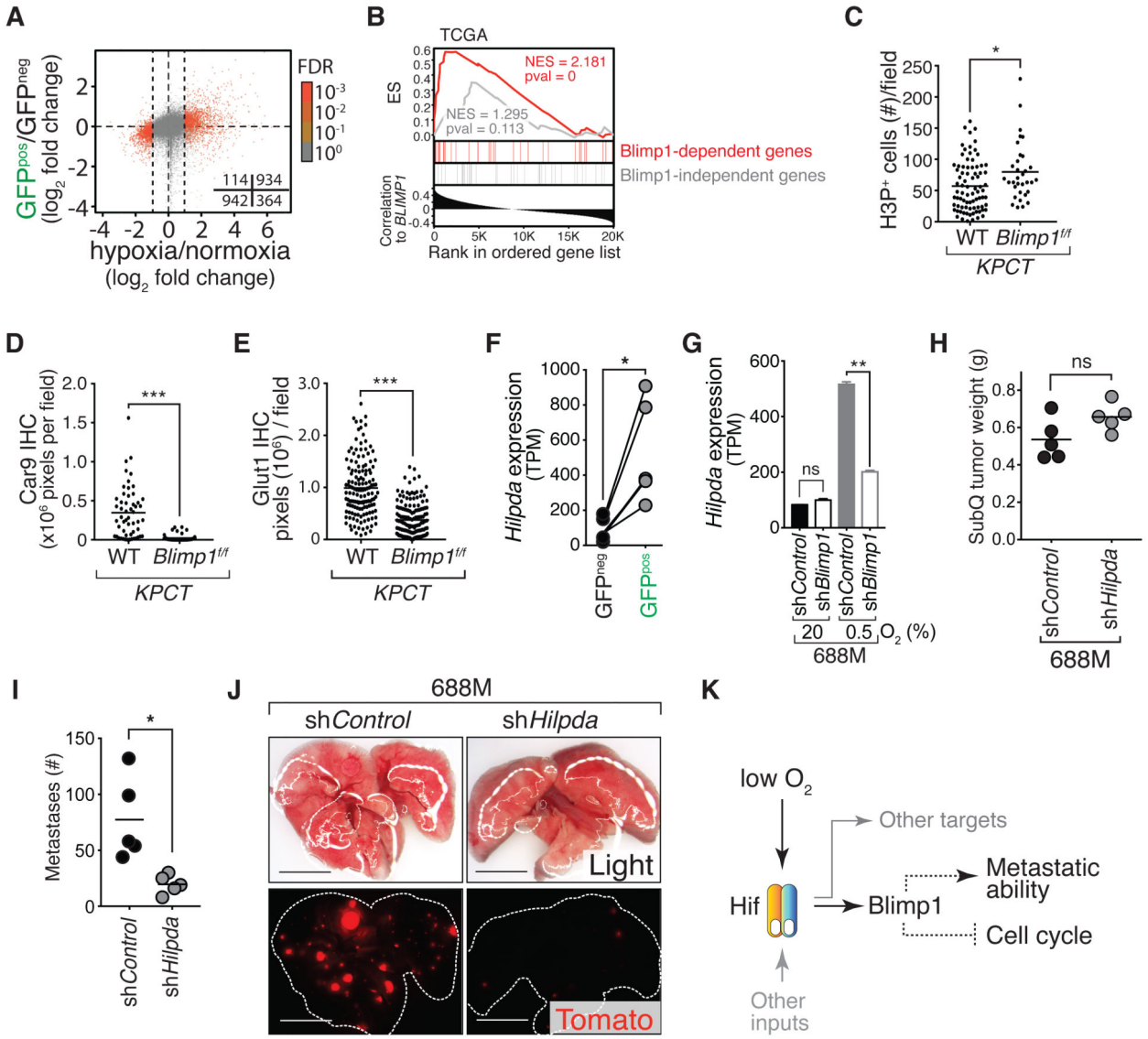

Figure 6. Blimp1 regulates the expression of pro-metastatic, hypoxia-induced target genes

(A) Genes that are significantly differentially expressed under hypoxia (absolute $\log_2$ fold change > 1 and FDR < 0.001) are differentially expressed between GFP^{pos} and GFP^{neg} cells (Fisher's exact test, quadrant counts shown, p-values < 0.0001).

(B) BLIMP1 expression correlates with a subset of hypoxia-induced genes in human PDAC. All genes from the TCGA PDAC dataset are ranked by their correlation with *BLIMP1* expression (Pearson r) and enrichments of 36 BLIMP1-dependent (red) and 36 BLIMP1-independent (grey), hypoxia-induced genes are shown. NS, enrichment score; NES, normalized enrichment score; pval, nominal p-value.

(C-E) *Blimp1* deficiency in *KPCT* mice significantly increases PDAC cell proliferation (C) while reduces Car9 (D) and Glut1 (E) expression (N = 3). Proliferation was measured by IHC for phospho-histone 3 (H3P). H3P positive nuclei were quantified. (C) Each dot is the number of $H3P^{pos}$ cells in a field and the bar is the mean. (D,E) Each dot is the sum of all

pixels (brown color) above the cutoff in a field and the bar is the mean. *, p-value < 0.05; ***, p-value < 0.0005 by Student's t test.

(F) Expression (TPM) of *Hilpda* in GFP^{pos} and GFP^{neg} PDAC cells from KPC^{colors} mice. Paired samples are connected with a line. *, p-value < 0.05 by paired t test.

(G) *Blimp1* knockdown significantly reduced hypoxia-induced *Hilpda* expression. **, p-value < 0.005. ns, not statistically significant.

(H-J) *Hilpda* is required for PDAC metastasis from subcutaneous tumors. (H) Each dot represents the mean of multiple subcutaneous tumor weight in a mouse and the bar is the mean of all mice in each cohort. (I) Each dot represents the number of lung metastases in a mouse and the bar is the mean. (J) Representative fluorescent images of lung metastases from the subcutaneous tumors are shown. Lung lobes are outlined with dotted lines (J). ns, not statistically significant; *, p-value < 0.05 by Student's t test. Scale bars = 0.5 cm.

(L) Proposed model. Dotted lines indicate potentially indirect mechanisms.